Angewandte Chemie
Eine Zeitschrift der Gesellschaft Deutscher Chemiker

Supporting Information

Revealing the Interfacial Chemistry of Fluoride Alkyl Magnesium Salts in Magnesium Metal Batteries

J. Long, S. Tan, J. Wang, F. Xiong, L. Cui, Q. An, L. Mai**

Supporting Information

69451 Weinheim, Germany

Revealing the Interfacial Chemistry of Fluoride Alkyl Magnesium Salts in Magnesium Metal Batteries

Juncai Long, Shuangshuang Tan, Junjun Wang, Fangyu Xiong, Lianmeng Cui, Qinyou An,* and Liqiang Mai*

DOI: 10.1002/anie.202301934

Experimental Procedures

Materials Synthesis

Synthesis of $Mg(OR^F)_2$ salts

All the reagents using in the synthesis were analytical grade and purchased from the Aladdin reagent Co., Ltd. Firstly, in an argon filled glovebox, perfluoro-tert-butyl alcohol ($(CF_3)_3COH$, 22 mmol) was dissolved in 10 mL dry 1,2-dimethoxyethane (DME), then, add 10 ml of Di-n-butyl magnesium ($[CH_3(CH_2)_3]_2Mg$, 10 mmol, 1.0 M in heptane) solution slowly to the above solution and stir overnight. Finally, the reaction product is removed from the solvent in vacuum to obtain white powder, which is $Mg(PFTB)_2$ salt. The $Mg(TFE)_2$ and $Mg(HFIP)_2$ samples were synthesized in the same procedure by regulating the $(CF_3)_3COH$ as 2,2,2-Trifluoroethanol (CF_3CH_2OH) and 1,1,1,3,3,3-Hexafluoro-2-propanol ($(CF_3)_2CHOH$), respectively.

Synthesis of electrolyte

In an argon filled glovebox, $AlCl_3$ (2 mmol) was dissolved in 5 mL dry DME. Then, $Mg(PFTB)_2$ (1 mmol) was added into the above solution. After magnetic stirring at room temperature for minutes, a clear solution was obtained. Finally, $MgCl_2$ (1 mmol) was added to the above solution and stirred at room temperature for 12 h to obtain a clear and colorless solution, which is MPFB electrolyte. MOME, MTFE and MHFP electrolytes were synthesized in the same procedure by regulating the $Mg(PFTB)_2$ as magnesium methanol ($Mg(OMe)_2$), $Mg(TFE)_2$ and $Mg(HFIP)_2$, respectively. MACC electrolyte was synthesized by stirring $AlCl_3$ (2 mmol) and $MgCl_2$ (2 mmol) in 5 mL dry DME obtained. $Mg(TFSI)_2$-based electrolyte was synthesized by stirring $Mg(TFSI)_2$ (2 mmol) in 4 mL dry DME or propylene carbonate (PC) obtained. All electrolytes are used directly, without any other purification steps.

Materials Characterizations

X-ray diffraction (XRD) patterns were collected using a D2 Advance X-ray diffractometer (Bruker) with a Cu Kα X-ray source. The crystals of MPFB electrolyte for single-crystals XRD studies were obtained by slowly evaporating the solvent in clear MPFB electrolyte. Data collection was collected at 100 K on a Bruker Smart Apex II diffractometer using Mo-Kα radiation (λ = 0.71073 Å). Calculations and refinement of structures were carried out using APEX2, SHELXTL, and Olex2 software. Fourier transform infrared (FTIR) spectra were measured by using Nicolet iS50 FTIR spectrometer in diffuse reflectance mode. X-ray photoelectron spectroscopy (XPS) measurements were carried out using Kratos Axis Supra XPS instrument. Field-emission scanning electron microscopy (FESEM) images were obtained by using JEOL-7100F microscope. Transmission electron microscopy (TEM) and high-resolution TEM (HRTEM) images, high-angle ring dark field image-scanning transmission electron microscope (HAADF-STEM) images, and energy dispersive spectroscopy (EDS) elemental mappings were recorded by using a Titan G2 60-300 microscope. ^{19}F and ^{13}C Nuclear Magnetic Resonance (NMR) spectra were collected using a Bruker 400 MHz, DMSO−d_6 spectrometer. Thermo Scientific Q Exactive Mass Spectrometer was used to quantitatively analyze the anion components in the electrolytes. TOF-SIMS measurements were conducted with a PHI nano TOF II. A Bi_3^{++} beam (30 keV, 2nA, 5 × 5 μm^2) was used as the primary beam to detect the samples, sputtering with an Ar^+ beam (3 keV, 100 nA, 400 × 400 μm^2) was applied for depth profiling analysis. The sputtering rate is ~0.17 nm/s on SiO_2.For the characterization of SEI, Mg||Mg symmetrical cells with different electrolytes were disassembled after 50 charge-discharge cycles at a current density of 0.5 mA cm^{-2}, 1 h charging and 1 h discharging. Then, the cycled Mg metal electrodes sample were rinsed with dry DME (1mL × 3 times) in glove box.

Electrochemical Measurement

CR2016 coin cells were assembled in an Ar-filled glove box with magnesium metal foil as the anode, glass fiber membrane (GF/A What-man) as the separator and MACC, MTFE, MHFP, MPFB as the electrolyte, respectively. The Mo_6S_8,[1] Mg_xMnO_2,[2] and CuS[3] powders were synthesized based on previous reports. The cathodes were prepared by spreading the mixed slurry composed of 70 wt% as-synthesized materials, 20 wt% super P, and 10 wt% polyvinylidene fluoride (PVDF) to stainless steel (SS) foils and dried at 70 °C. The mass loading of the active material is about 1.5 mg cm^{-2}. Mg_xMnO_2 cathodes were obtained with 50% as synthesized active materials, 40% acetylene black and 10% PTFE. The loading of the active material was about 5–7mg cm^{-2}.The electrochemical performance of the batteries was performed by using a multi-channel battery test system (LAND CT2001A). CE measurements were conducted using asymmetric Mg||Cu cells. The cells were discharged for 30 minutes and charge to 1.5 V at a current density of 0.5 mA cm^{-2}. Symmetric Mg||Mg cells were assembled for evaluating the polarization properties of the electrolytes. Cyclic voltammetry (CV) curves, linear scan voltammetry (LSV) and electrochemical impedance spectroscopy (EIS) plots were tested using a BioLogic VMP3 multichannel electrochemical workstation. The CV was studied by a three-electrode system using Mg as the reference and counter electrode and Mo as the working electrode at a scanning rate of 25 mV s^{-1}. LSV was carried out using Al, Cu, SS, Ti and Mo foils as the working electrode and Mg foil as the reference and counter electrode. The scan rate was 10 mV s^{-1}. Electrochemical impedance spectroscopy (EIS) characterization of symmetric Mg||Mg cells were assembled for evaluating the interfacial impedance change before and after electrochemical cycling. The ionic conductivity (σ) of SEI was calculated according to Equation (1), which S is the effective contacting area, R presents the resistance value of the SEI layer, and L the thickness of the SEI.

$$\sigma = \frac{L}{S \cdot R} \quad (1)$$

Theoretical Calculation

MD simulations were carried out to explore the coordination environment of the electrolyte systems. The simulations were performed with the help of Forcite package in Materials Studio. The COMPASSIII force field (Condensed-phase Optimized Molecular

SUPPORTING INFORMATION

Potentials for Atomistic Simulation Studies) that enables accurate prediction of a broad range of molecules and polymers properties was selected for the prediction of the solvent structures of the studied systems. The electrostatic and van der Waals interactions in the systems were described by Ewald summation method. The initial configurations were first relaxed with the max iterations of 5000 steps. The obtained configurations were annealed with the temperature range of 300 to 1000 K, and the heating ramps per cycle and dynamics step per ramp were respectively set to 5 and 1000. The systems were then pre-equilibrated via NPT ensemble at 300 K, the time step and total simulation time were set to 1.0 fs and 1000 ps, respectively. Another NVT process with simulation time of 1000 ps was performed for the statistic analysis of RDF (radial distribution function). All calculations and further model optimization are run on Gaussian 09 package and calculated on the basis of M062X/6-311+G. The electrostatic potential (ESP) and orbital composition analysis of the highest occupied molecular orbital/lowest unoccupied molecular orbital (HOMO/LUMO) were derived from the optimized structure. The visualization of theoretical calculations was conducted by Visual Molecular Dynamics (VMD) and Multiwfn.

Results and Discussion

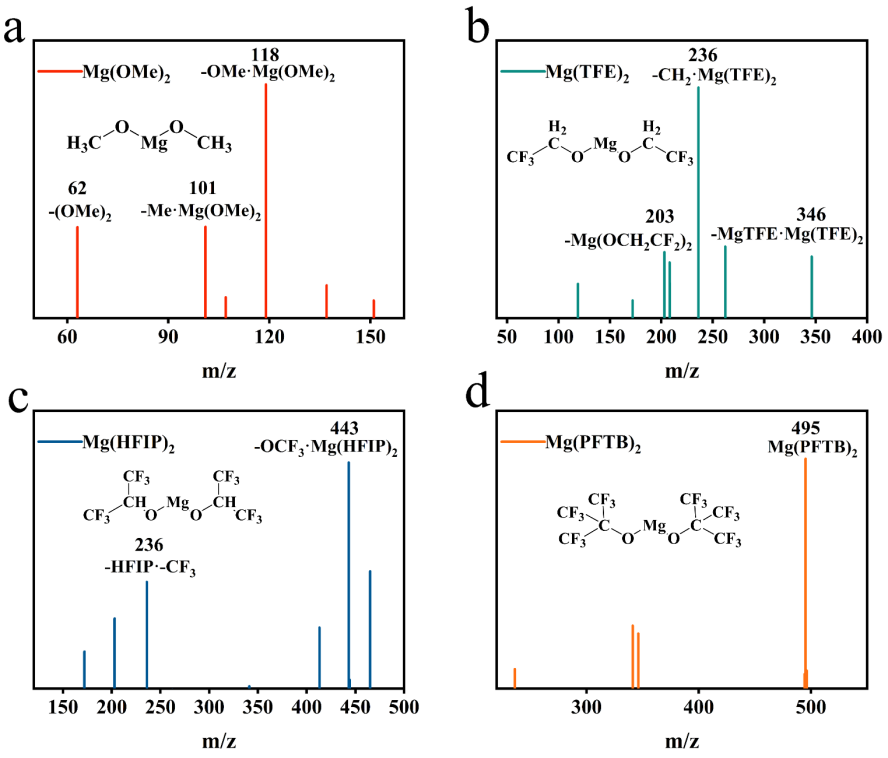

Figure S1. MS results and structural formulas of the (a) $Mg(OMe)_2$, (b) $Mg(TFE)_2$, (c) $Mg(HFIP)_2$, and (d) $Mg(PFTB)_2$ salts.

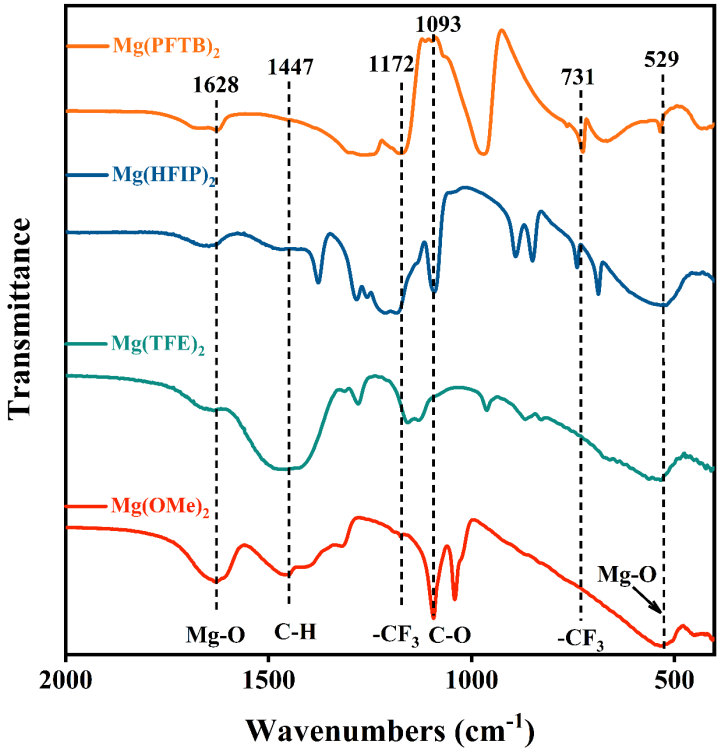

Figure S2. FTIR spectrum of $M(OMe)_2$, $Mg(TFE)_2$, $Mg(HFIP)_2$, and $Mg(PFTB)_2$ salts.

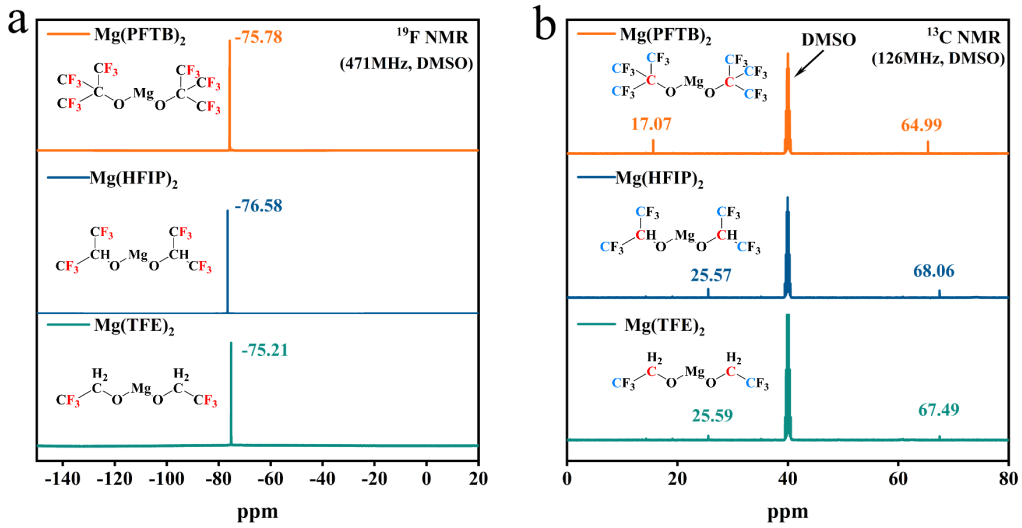

Figure S3. (a) ^{19}F NMR spectrum and (b) ^{13}C NMR spectrum of $Mg(TFE)_2$, $Mg(HFIP)_2$, and $Mg(PFTB)_2$ salts in DMSO solvent.

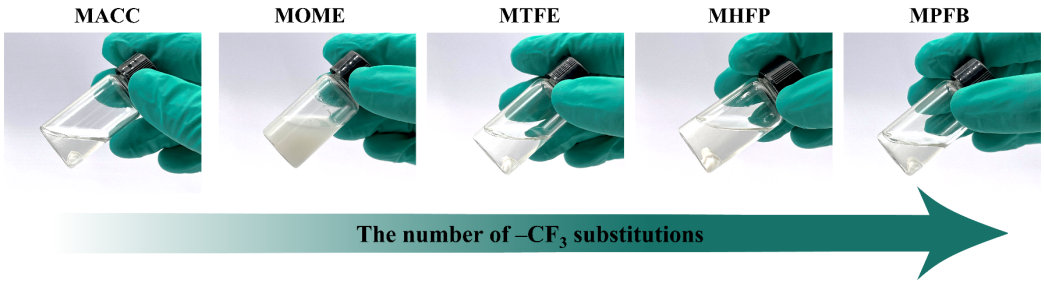

Figure S4. Optical photographs of MACC, MOME, MTFE, MHFP, and MPFB electrolytes.

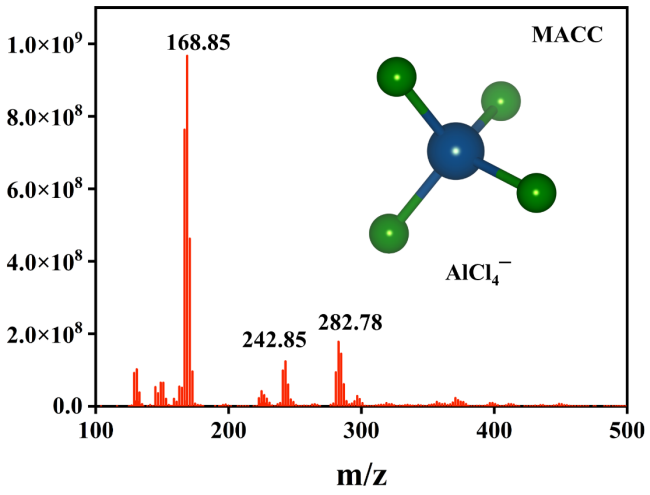

Figure S5. MS results of the MACC electrolyte.

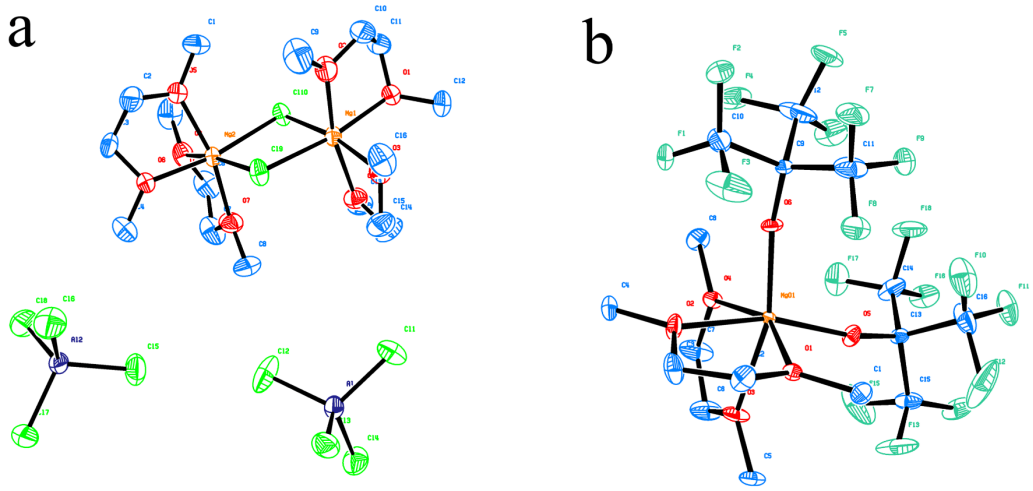

Figure S6. ORTEP plots of the coordination structure of crystallized (a) $[Mg_2Cl_2{\cdot}4DME][AlCl_4]_2$ and (b) $[Mg{\cdot}2DME][PFTB]_2$ the thermal ellipsoid is shown at 40% probability.

Crystal Data for $C_{16}H_{40}O_8Mg_2Al_2Cl_{10}$ and $C_{16}H_{20}O_6MgF_{18}$

The CIF files have been deposited in the Cambridge Crystallographic Data Centre (CCDC) with deposition numbers 2245737 and 2245740.

Table S1. Crystal data and structure refinement for **$[Mg_2Cl_2 \cdot 4DME][AlCl_4]_2$**

Empirical formula	$C_{16}H_{40}O_8Mg_2Al_2Cl_{10}$
Formula weight	817.6
Temperature/K	100.15
Crystal system	orthorhombic
Space group	Pca21
a/Å	26.5608(7)
b/Å	7.2850(2)
c/Å	19.0790(5)
α/°	90
β/°	90
γ/°	90
Volume/$Å^3$	3691.70(17)
Z	35
$\rho_{calc}g/cm^3$	1.471
μ/mm^{-1}	0.871
F (000)	1680.0
Crystal size/mm^3	2 × 2 × 2
Radiation	Mo Kα (λ = 0.71073)
2θ range for data collection/°	4.27 to 71.61
Index ranges	$-35 \leq h \leq 40$, $-11 \leq k \leq 11$, $-29 \leq l \leq 29$
Reflections collected	42562
Independent reflections	14524 [R_{int} = 0.0490, R_{sigma} = 0.0583]
Data/restraints/parameters	14524/1/351
Goodness-of-fit on F^2	1.064

Table S2. Crystal data and structure refinement for **[Mg·2DME][PFTB]$_2$**

Empirical formula	$C_{16}H_{20}O_6MgF_{18}$
Formula weight	674.6
Temperature/K	296.15
Crystal system	monoclinic
Space group	C2/c
a/Å	28.913(18)
b/Å	10.579(6)
c/Å	17.472(10)
α/°	90
β/°	17.472(10)
γ/°	90
Volume/Å^3	5244(5)
Z	86
ρ_{calc}g/cm^3	1.658
μ/mm^{-1}	0.224
F (000)	2544.0
Crystal size/mm^3	2 × 2 × 2
Radiation	Mo Kα (λ = 0.71073)
2θ range for data collection/°	2.87 to 55.372
Index ranges	$-37 \leq h \leq 22$, $-13 \leq k \leq 13$, $-22 \leq l \leq 21$
Reflections collected	17280
Independent reflections	6020 [R_{int} = 0.0648, R_{sigma} = 0.0834]
Data/restraints/parameters	6020/0/370
Goodness-of-fit on F^2	1.437

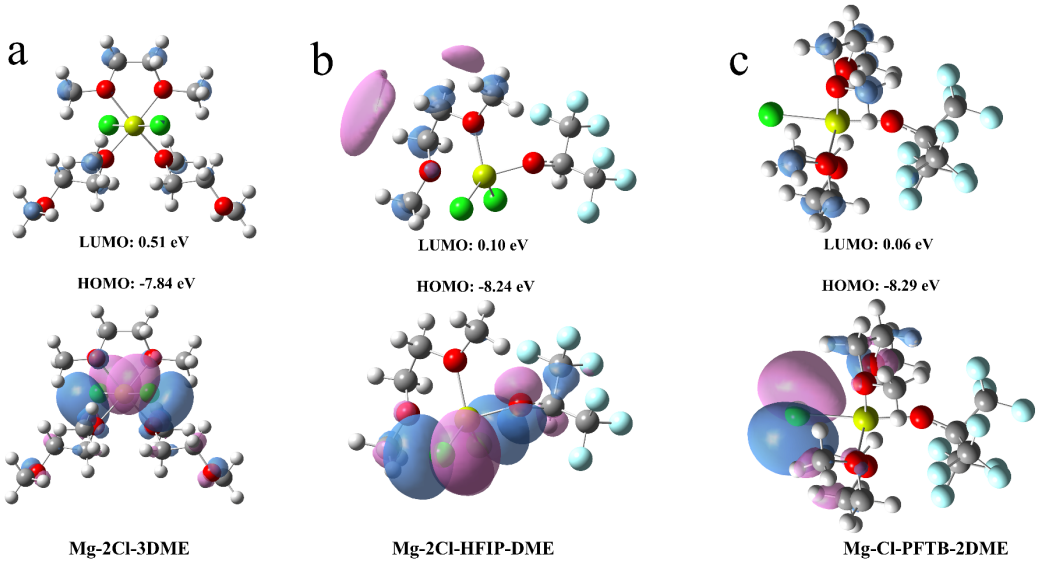

Figure S7. LUMO and HOMO energy of the local coordination structure of Mg^{2+} in various electrolytes obtained by DFT calculations, (a) Mg-2Cl-3DME, (b) Mg-2Cl-HFIP-DME, (c) Mg-Cl-PFTB-2DME. White, grey, blue, red, green, and yellow balls represent H, C, F, O, Cl, and Mg atoms, respectively. Blue and purple regions represent the positive and negative parts of orbitals, respectively.

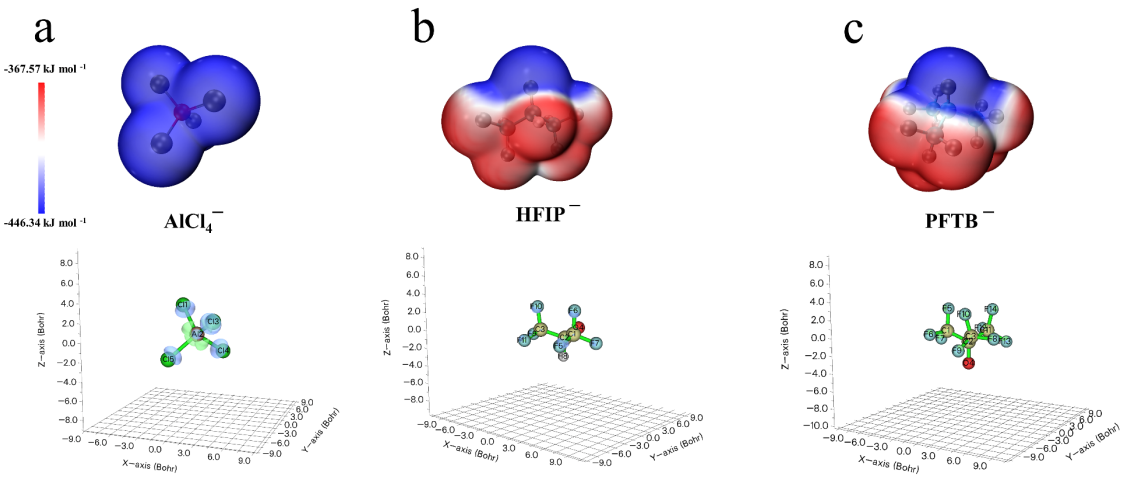

Figure S8. Electrostatic potential maps (ESP) and natural bond orbitals (NBO) of (a) [$AlCl_4^-$], (b) [$HFIP^-$], and (c) [$PFTB^-$] anions.

Table S3. The values of different anionic dipole moments

Anion	Magnitude	Vector		
		X	Y	Z
$AlCl_4^-$	0.0029	0.0009	-0.0017	0.0022
$HFIP^-$	5.0278	-0.0002	-4.8376	-1.3700
$PFTB^-$	3.9651	-0.0010	0.0012	3.9651

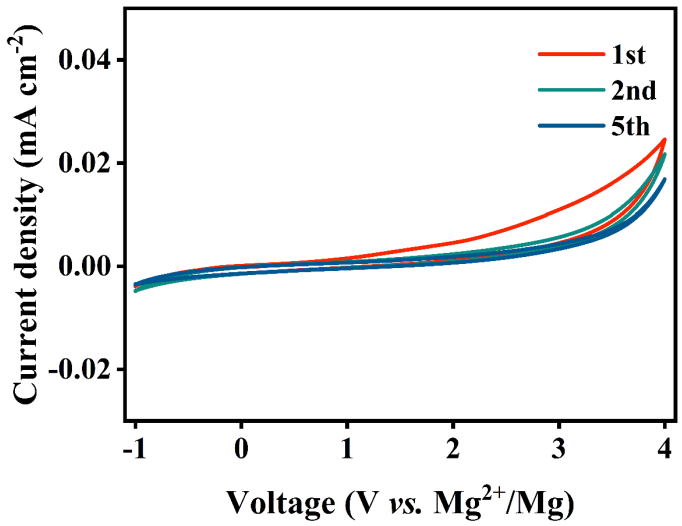

Figure S9. Cyclic voltammograms of the Mg plating and stripping process using MOME electrolyte. No reversible plating-stripping behaviour was observed.

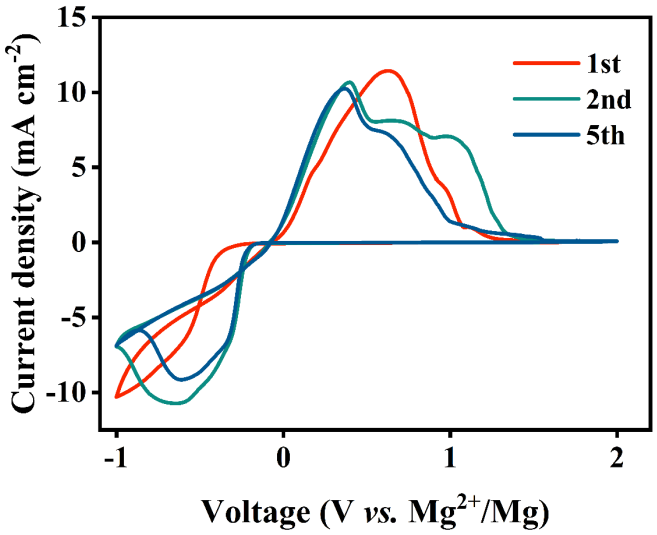

Figure S10. Cyclic voltammograms of the Mg plating and stripping process using MACC electrolyte. The appearance of the two deposition peaks is due to the irreversible deposition process of Al in the early stage.

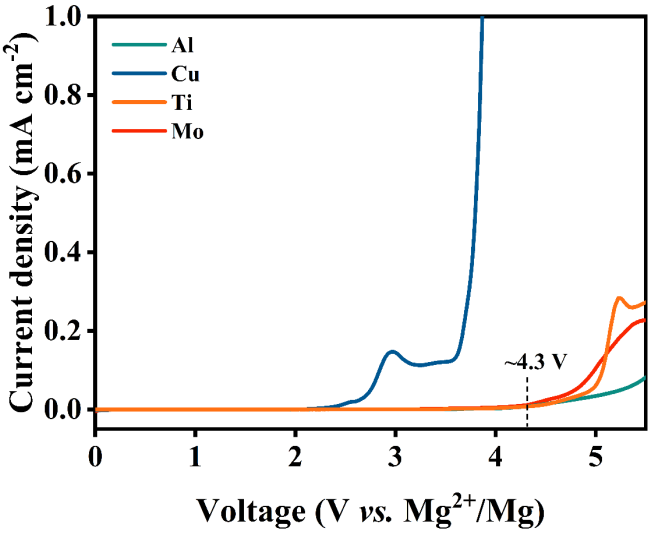

Figure S11. Oxidation stability of 0.5 M $Mg(PFTB)_2$-DME in different metal electrodes tested by LSV.

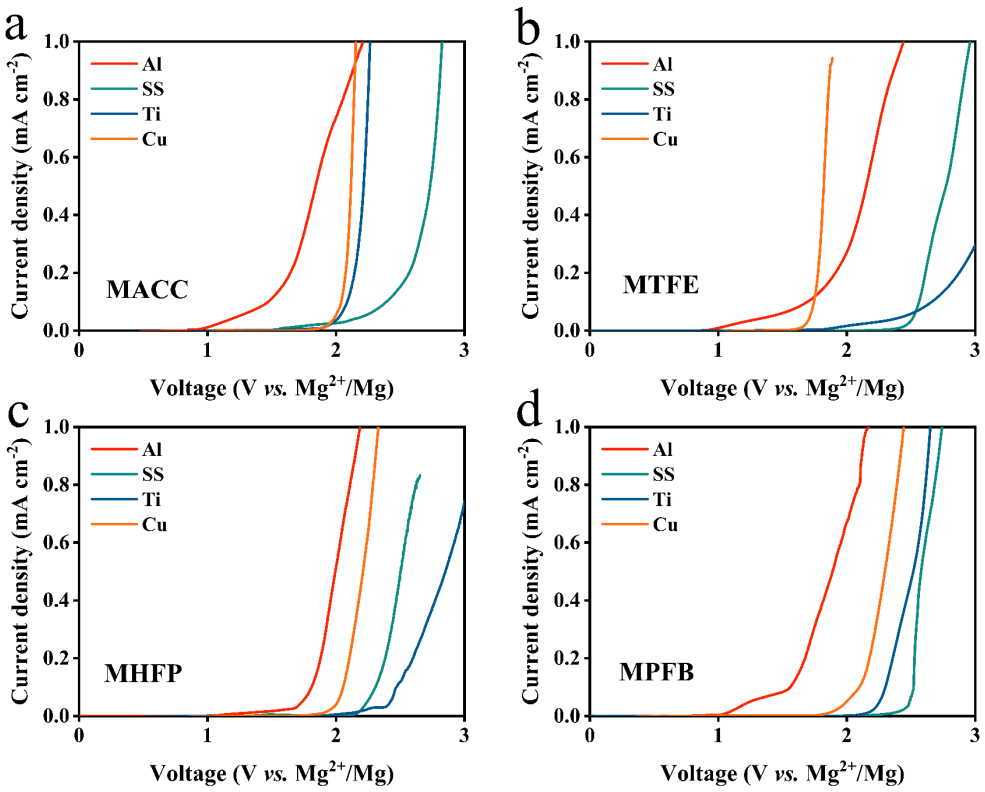

Figure S12. Oxidation stability of (a) MACC, (b) MTFE, (c) MHFP, and (d) MPFB electrolytes in different metal electrodes tested by LSV.

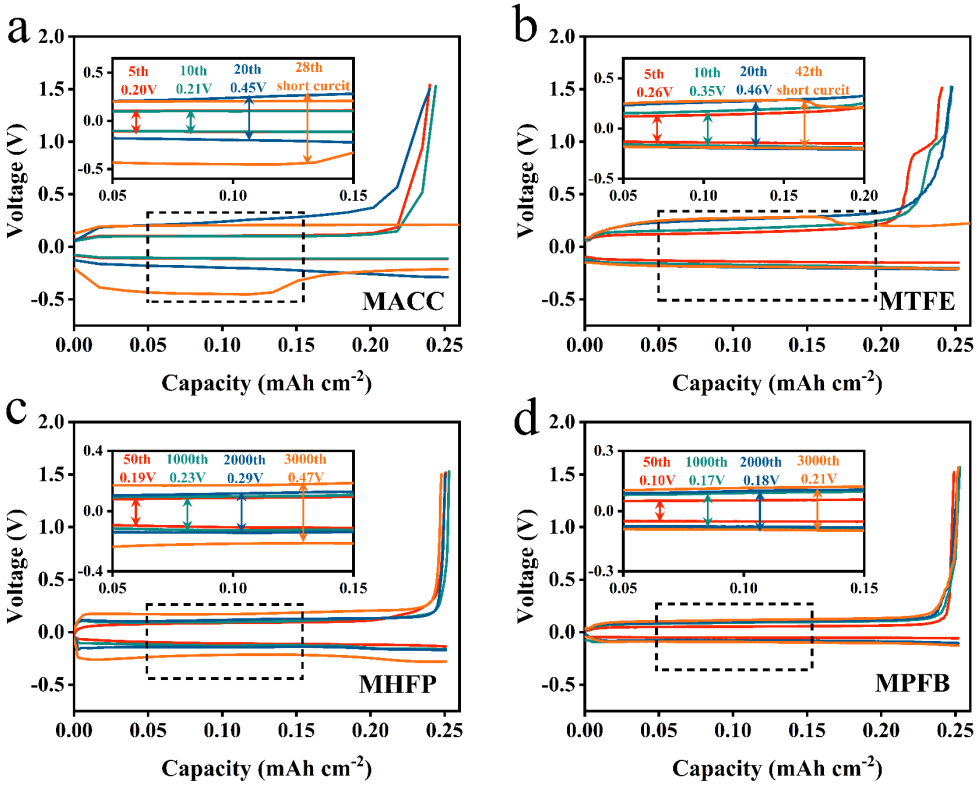

Figure S13. Corresponding voltage profiles of Mg plating and stripping process in (a) MACC, (b) MTFE, (c) MHFP, and (d) MPFB electrolytes. Insets show an enlarged view at the cycles framed by the four dashed rectangles.

Table S4. Performance comparison of the reported electrolytes with this work.

Electrolyte	Current density (mA cm^{-2})	Areal capacity (mAh cm^{-2})	Cycle time (h)	Overpotential (mv)	References
$Mg(TFSI)_2$+ $GeCl_4$	0.02	0.005	1000	~250	[4]
MLCC	0.5	0.5	500	~140	[5]
$Li[B(hfip)_4]$	1	0.5	2000	~220	[6]
Mg-FPB	0.1	/	500	~50	[7]
$Mg(OTf)_2$ +$InCl_3$	0.5	0.5	600	~150	[8]
$Mg(HMDS)_2$+ $TBABH_4$	0.5	0.5	2000	~250	[9]
$Mg[B(hfip)_4]_2$	0.1	0.05	1200	~100	[10]
$[Mg\text{-}(THF)_6]$ $[AlCl_4]_2$	0.05	0.0125	50	~300	[11]
OMBB	0.1	0.05	700	~40	[12]
MTB	0.05	0.05	200	~250	[13]
MHFP (this work)	0.5	0.5	2000	120	/
MPFB (this work)	**0.5**	**0.5**	**2000**	**50**	/

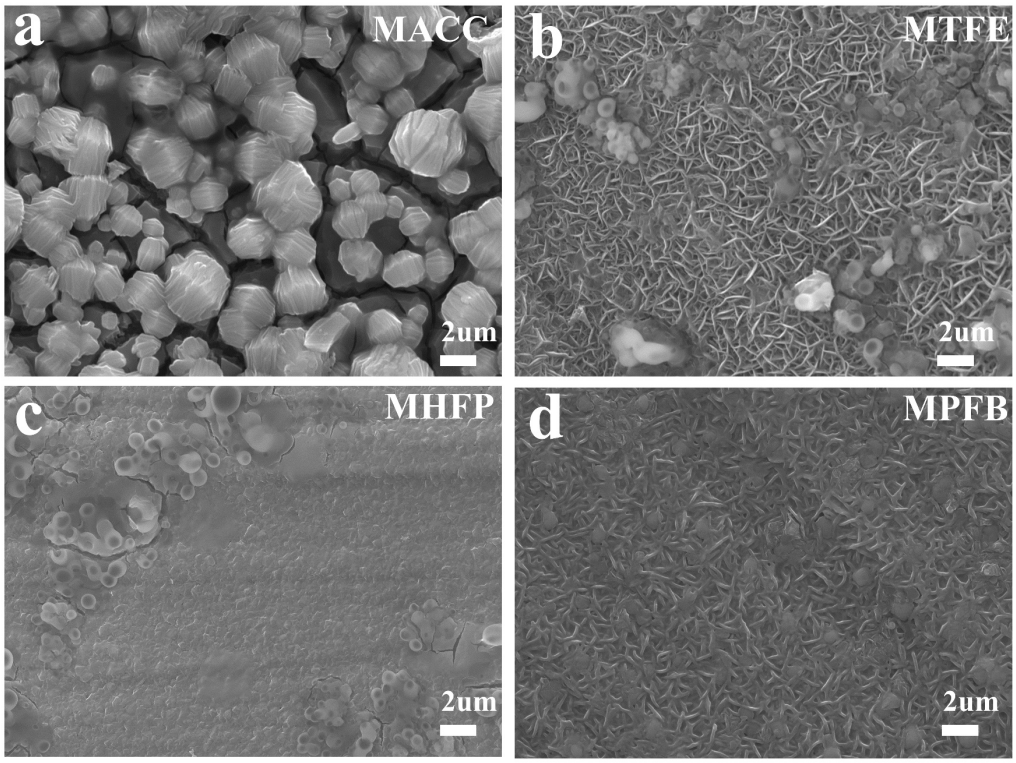

Figure S14. Typical SEM images of the Mg deposits at (a) MACC, (b) MTFE, (c) MHFP, and (d) MPFB electrolytes. The deposited Mg was obtained by discharging at 0.5 mA^{-2} for 2 hours in Mg||Cu asymmetric cell.

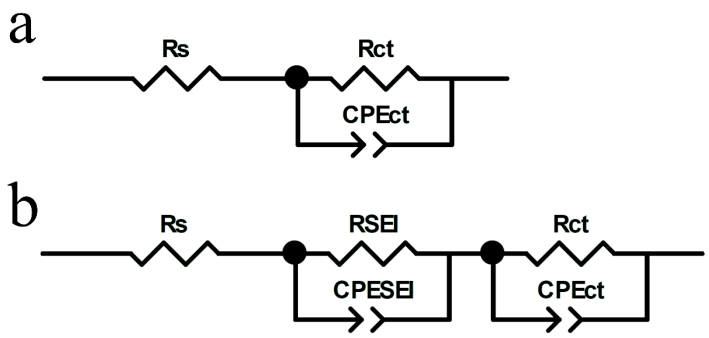

Figure S15. The equivalent circuits employed to analyze the EIS curves (a) before and (b) after cycle, in which Rs indicates the system resistance, CPE is the constant phase element; R_{SEI} is corresponding to the resistance of ion migration in SEI, R_{ct} stands for the charge transfer resistance.

Table S5. The fitted parameters of the *in-situ* EIS results cycled in Mg||Mg symmetric cell for different electrolytes.

Electrolyte	Fitted parameters	Before cycle	After 5th cycle	After 10th cycle	After 20th cycle
MACC	$R_s(\Omega)$	6.2	12.5	14.9	17.9
	$R_{ct}(\Omega)$	688.8	91.7	61.9	61.2
	$R_{SEI}(\Omega)$	/	/	/	/
MTFE	$R_s(\Omega)$	17.9	78.9	90.6	132
	$R_{ct}(\Omega)$	8206	168.7	172.8	216.4
	$R_{SEI}(\Omega)$	/	13.8	12.7	11.26
MHFP	$R_s(\Omega)$	5.3	8.2	9.6	8.2
	$R_{ct}(\Omega)$	2558	308.8	172.9	432.4
	$R_{SEI}(\Omega)$	/	24.6	10.3	13.24
MPFB	$R_s(\Omega)$	3.5	5.8	6.8	6.8
	$R_{ct}(\Omega)$	1437	260.5	190.3	265.6
	$R_{SEI}(\Omega)$	/	25.3	14.2	10.4

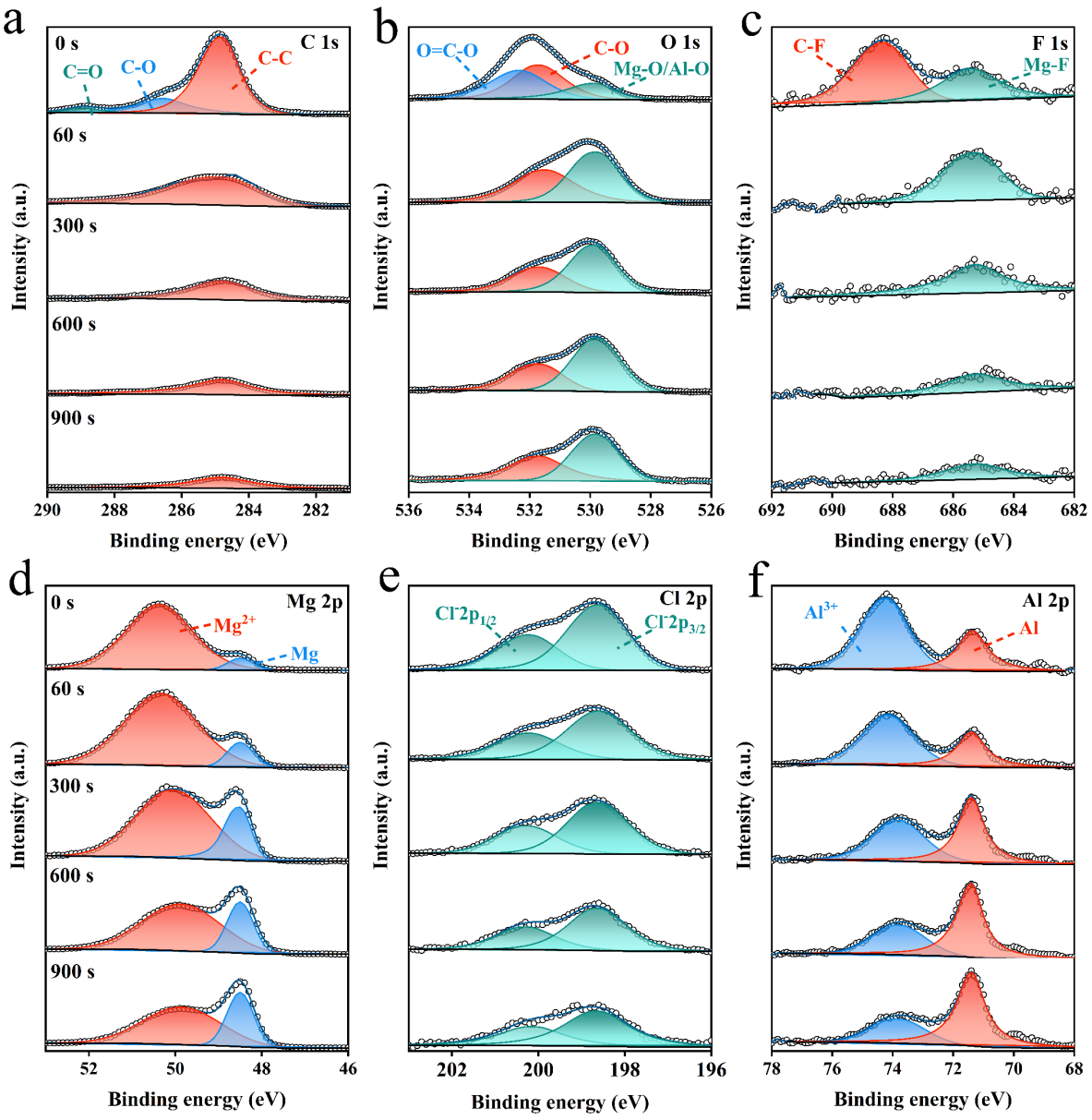

Figure S16. XPS etching analysis of the Mg anode after cycling in MTFE electrolyte, (a) C 1s, (b) O 1s, (c) F 1s, (d) Mg 2p, (e) Cl 2p, and (f) Al 2p.

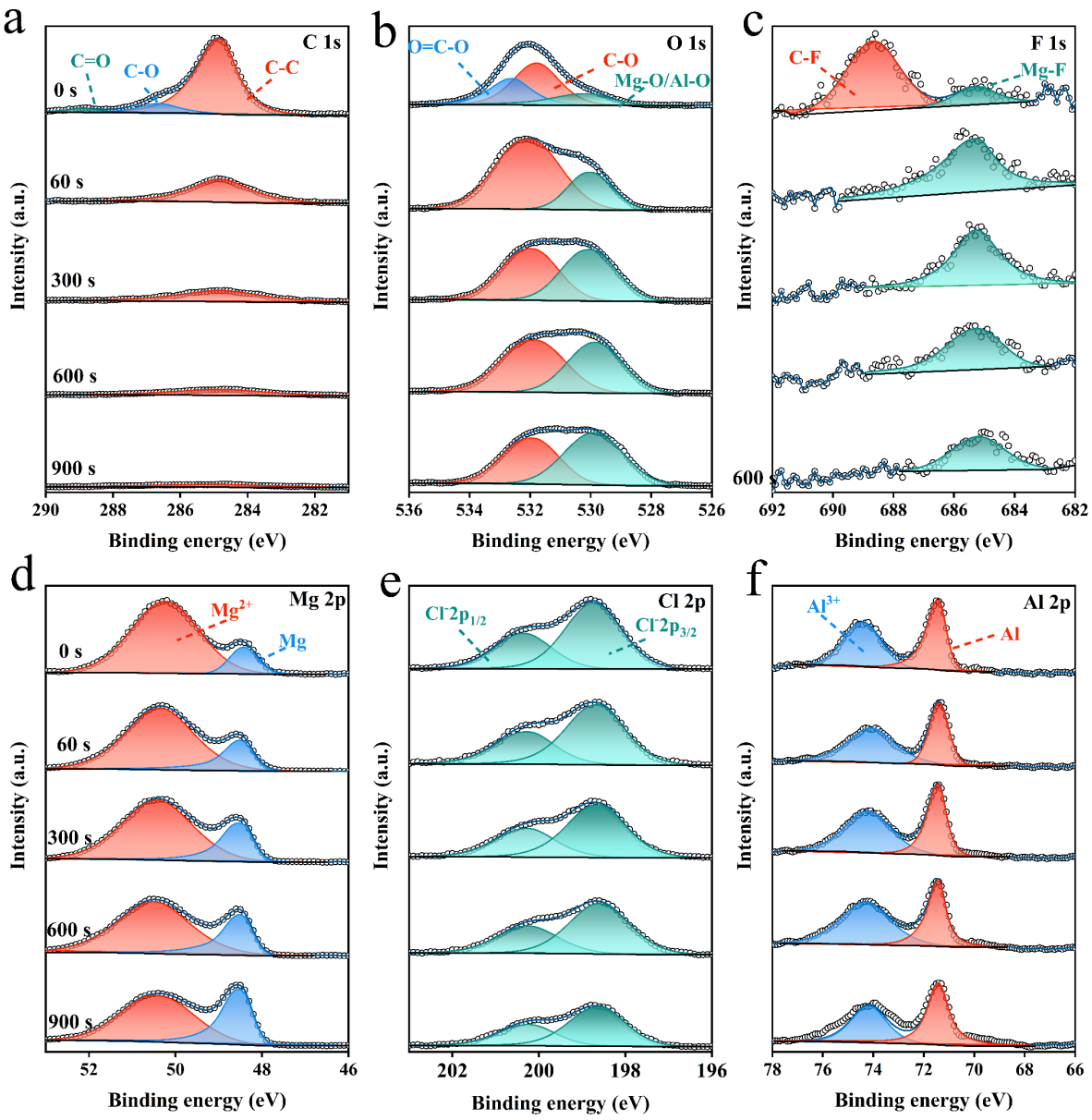

Figure S17. XPS etching analysis of the Mg anode after cycling in MHFP electrolyte, (a) C 1s, (b) O 1s, (c) F 1s, (d) Mg 2p, (e) Cl 2p, and (f) Al 2p.

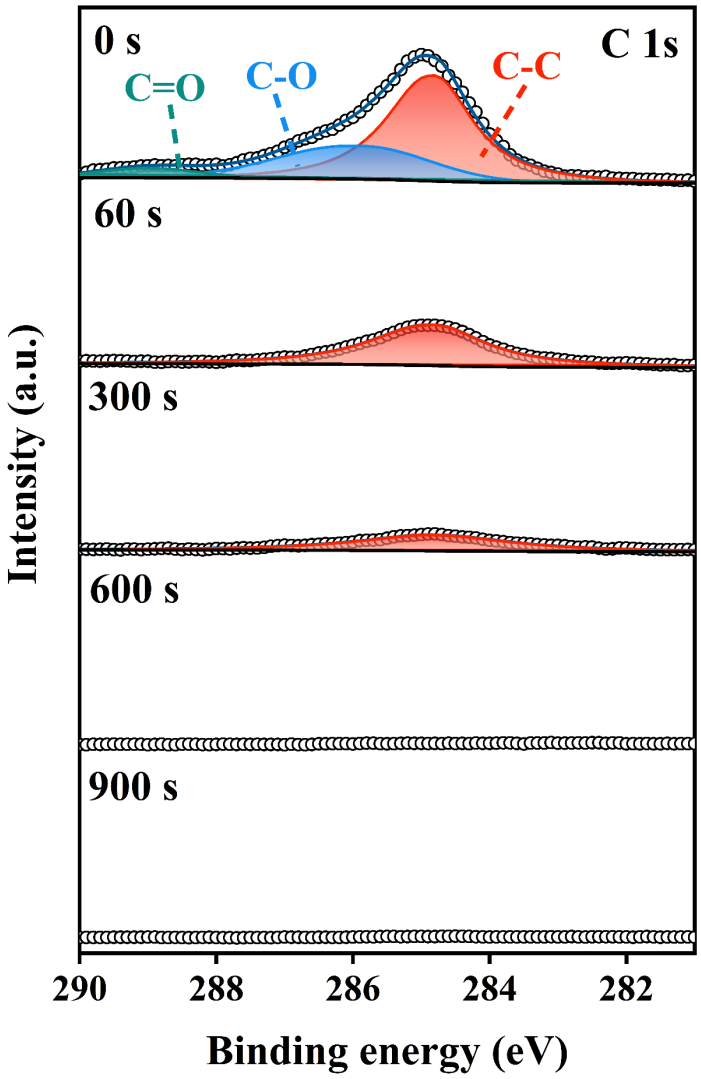

Figure S18. XPS C 1s spectrum etching analysis of the Mg anode after cycling in MPFB electrolyte.

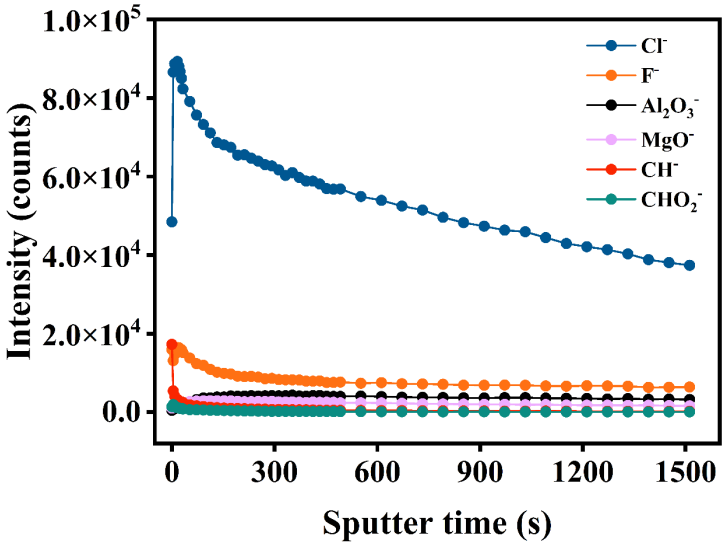

Figure S19. TOF-SIMS depth profiles of CH^-, CHO_2^-, MgO^-, $Al_2O_3^-$, Cl^-, F^- for the cycled Mg anode in MPFB electrolyte.

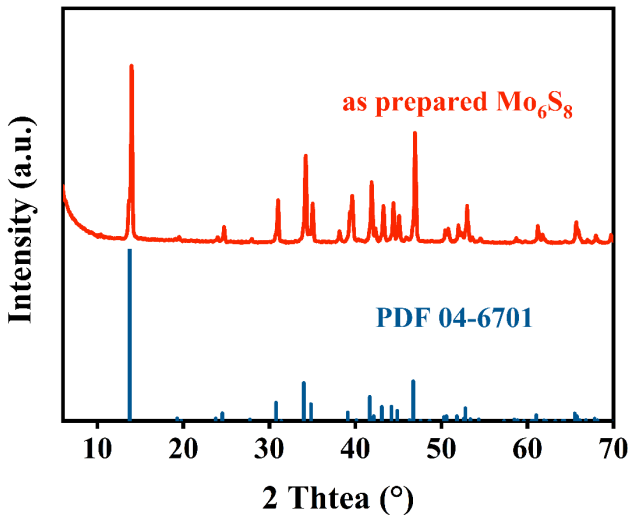

Figure S20. The XRD pattern of Mo_6S_8 cathode.

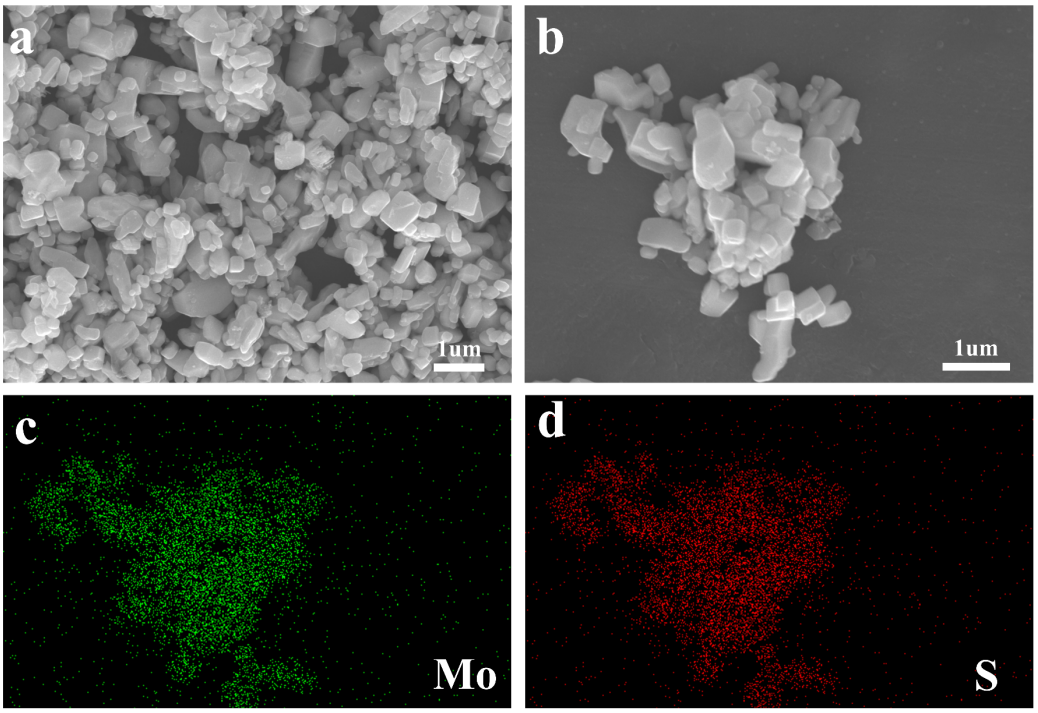

Figure S21. (a, b) SEM images and (c, d) EDS elemental mappings of Mo_6S_8 cathode.

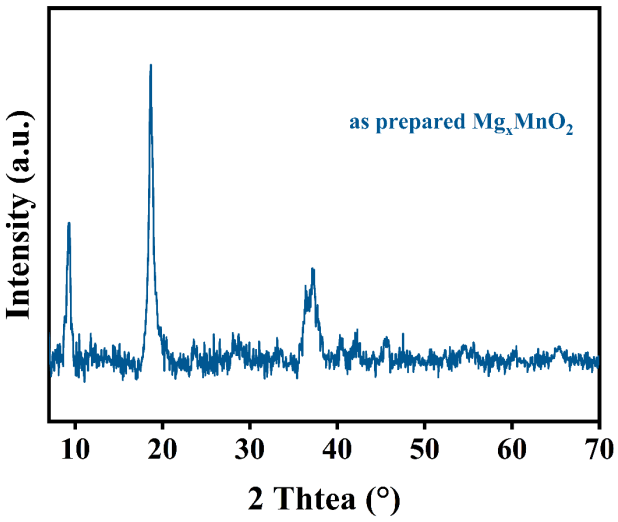

Figure S22. The XRD pattern of Mg_xMnO_2 cathode.

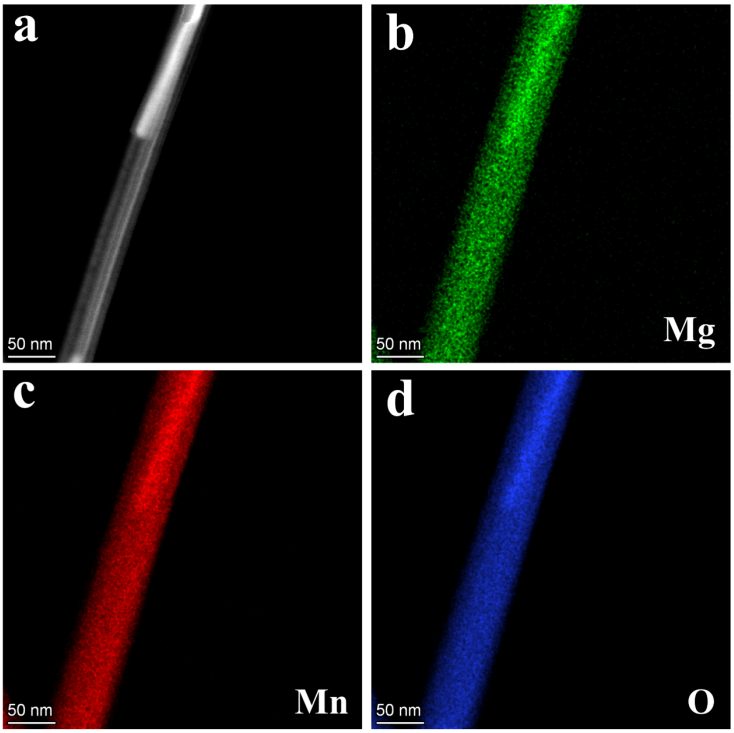

Figure S23. HAADF-STEM image and EDS elemental mappings of Mg_xMnO_2 cathode.

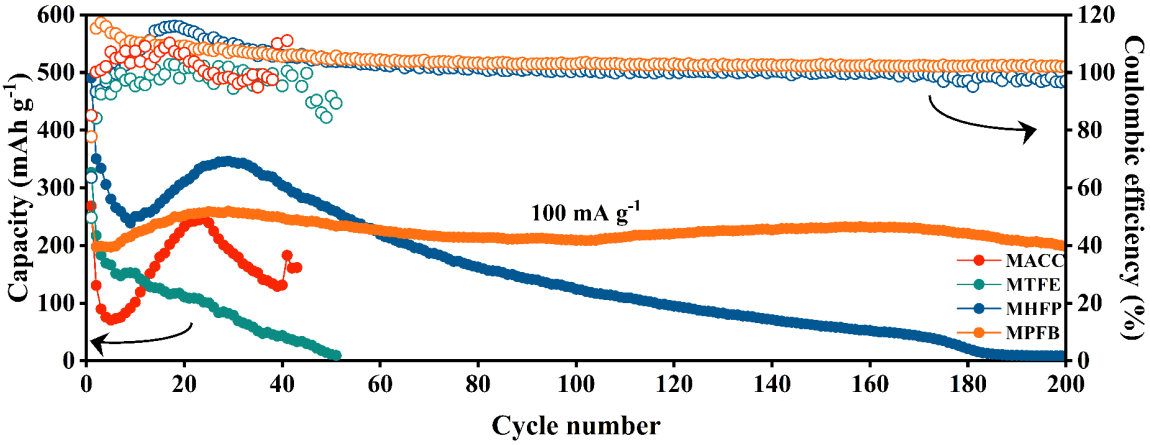

Figure S24. Long-term cycling performance of different electrolytes in CuS cathode.

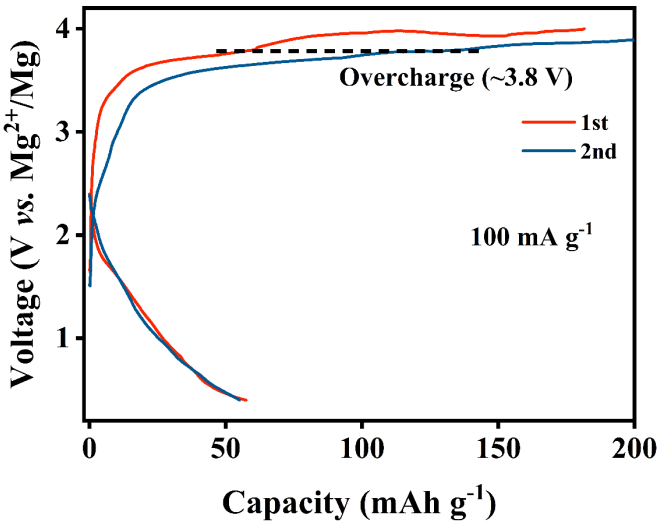

Figure S25. Electrochemical performance of Mg||Mg_xMnO_2 battery using MPFB electrolyte between 0.4~4 V.

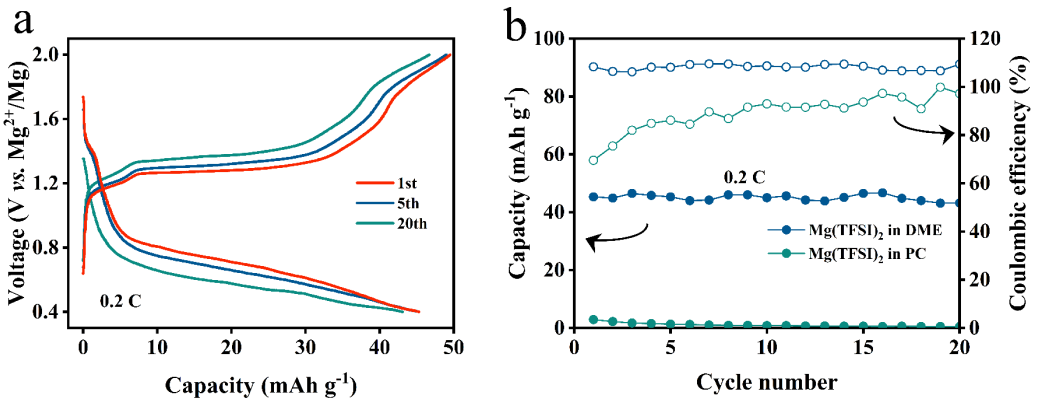

Figure S26. (a) Electrochemical performance of Mg||Mo_6S_8 battery using Mg(TFSI)$_2$-DME electrolyte, where the anode are the cycled Mg anode from MPFB electrolyte, (b) Cycling performances of Mg||Mo_6S_8 batteries using Mg(TFSI)$_2$-DME and Mg(TFSI)$_2$-PC electrolytes.

References

[1] Y. Cheng, L. R. Parent, Y. Shao, C. Wang, V. L. Sprenkle, G. Li, J. Liu, *Chem. Mater.* **2014**, *26*, 4904-4907.
[2] Z. Yang, X. Pan, Y. Shen, R. Chen, T. Li, L. Xu, L. Mai, *Small* **2022**, *18*, 2107743.
[3] W. Ren, F. Xiong, Y. Fan, Y. Xiong, Z. Jian, *ACS Appl. Mater. Interfaces* **2020**, *12*, 10471-10478.
[4] J. Zhang, X. Guan, R. Lv, D. Wang, P. Liu, J. Luo, *Energy Storage Mater.* **2020**, *26*, 408-413.
[5] H. Fan, Z. Zheng, L. Zhao, W. Li, J. Wang, M. Dai, Y. Zhao, J. Xiao, G. Wang, X. Ding, H. Xiao, J. Li, Y. Wu, Y. Zhang, *Adv. Funct. Mater.* **2020**, *30*, 1909370.
[6] K. Tang, A. Du, S. Dong, Z. Cui, X. Liu, C. Lu, J. Zhao, X. Zhou, G. Cui, *Adv. Mater.* **2020**, *32*, 1904987.
[7] J. Luo, Y. Bi, L. Zhang, X. Zhang, T. L. Liu, *Angew. Chem., Int. Ed.* **2019**, *58*, 6967-6971.
[8] G. Yang, Y. Li, C. Zhang, J. Wang, Y. Bai, C. Y. J. Lim, M.-F. Ng, Z. Chang, S. Kumar, Z. Sofer, W. Liu, Z. W. Seh, *Nano Lett.* **2022**, *22*, 9138–9146.
[9] R. Horia, D. T. Nguyen, A. Y. S. Eng, Z. W. Seh, *Nano Lett.* **2021**, *21*, 8220-8228.
[10] Z. Zhao-Karger, R. Liu, W. Dai, Z. Li, T. Diemant, B. P. Vinayan, C. Bonatto Minella, X. Yu, A. Manthiram, R. J. Behm, M. Ruben, M. Fichtner, *ACS Energy Lett.* **2018**, *3*, 2005-2013.
[11] W. Li, S. Cheng, J. Wang, Y. Qiu, Z. Zheng, H. Lin, S. Nanda, Q. Ma, Y. Xu, F. Ye, M. Liu, L. Zhou, Y. Zhang, *Angew. Chem., Int. Ed.* **2016**, *55*, 6406-6410.
[12] A. Du, Z. Zhang, H. Qu, Z. Cui, L. Qiao, L. Wang, J. Chai, T. Lu, S. Dong, T. Dong, H. Xu, X. Zhou, G. Cui, *Energy Environ. Sci.* **2017**, *10*, 2616-2625.
[13] D. Huang, S. Tan, M. Li, D. Wang, C. Han, Q. An, L. Mai, *ACS Appl. Mater. Interfaces* **2020**, *12*, 17474-17480.

Author Contributions

J. Long: Conceptualization (lead), Data curation (lead), Resources (lead), Software (lead), Writing-original draft (lead); S. Tan: Writing-review editing(equal), formal analysis (equal); J. Wang: Writing-review editing(equal); L. Cui: Validation (equal); F. Xiong: Writing-review editing(equal); Q. An: Conceptualization (equal), Investigation (lead), Funding acquisition (lead), Writing-review editing(lead); L. Mai: Conceptualization (lead), Supervision (lead), Funding acquisition (lead), Writing-review editing(lead).